

# Atomic mutagenesis of $N^6$ -methyladenosine reveals distinct recognition modes by human $m^6A$ reader and eraser proteins

Florian Seitz<sup>†</sup>, Tina Jungnickel<sup>†</sup>, Nicole Kleiber<sup>‡</sup>, Jens Kretschmer<sup>‡</sup>, Julia Dietzsch<sup>†</sup>, Juliane Adelmann<sup>†</sup>, Katherine E. Bohnsack<sup>‡</sup>, Markus T. Bohnsack<sup>‡,1</sup>, and Claudia Höbartner<sup>\*,†,#</sup>.

<sup>†</sup>Institute of Organic Chemistry, University of Würzburg, Am Hubland, 97074 Würzburg, Germany. <sup>‡</sup>Department of Molecular Biology, University Medical Centre Göttingen, Humboldtallee 23, 37073 Göttingen, Germany. <sup>1</sup>Göttingen Center for Molecular Biosciences, Georg-August University Göttingen, Justus-von-Liebig-Weg 11, 37077 Göttingen, Germany. <sup>#</sup> Center for Nanosystems Chemistry, University of Würzburg, Theodor-Boveri-Weg, 97074 Würzburg, Germany.

**ABSTRACT:**  $N^6$ -methyladenosine ( $m^6A$ ) is an important modified nucleoside in cellular RNA associated with multiple cellular processes and implicated in diseases. The enzymes associated with the dynamic installation and removal of  $m^6A$  are heavily investigated targets for drug research, which requires detailed knowledge of the recognition modes of  $m^6A$  by proteins. Here we use atomic mutagenesis of  $m^6A$  to systematically investigate the mechanisms of the two human  $m^6A$  demethylase enzymes FTO and ALKBH5 and the binding modes of YTH reader proteins YTHDF2/DC1/DC2. Atomic mutagenesis refers to atom-specific changes that are introduced by chemical synthesis, such as replacement of nitrogen by carbon atoms. Synthetic RNA oligonucleotides containing site-specifically incorporated 1-deaza-, 3-deaza-, and 7-deaza- $m^6A$  nucleosides were prepared by solid-phase synthesis and their RNA binding and demethylation by recombinant proteins were evaluated. We found distinct differences in substrate recognition and transformation and revealed structural preferences for enzymatic activity. The deaza  $m^6A$  analogues introduced in this work will be useful probes for other proteins in  $m^6A$  research.

## Introduction

$N^6$ -methyladenosine ( $m^6A$ ) is an important modified nucleoside found at internal positions in various types of RNAs, predominantly in eukaryotic mRNAs and also in non-coding RNAs.<sup>1-6</sup> The methyl group is enzymatically installed by *S*-adenosylmethionine (SAM)-dependent methyltransferases, such as the multi-component METTL3/14  $m^6A$  writer complex, which targets adenosines in a subset of consensus DRACH (D=A/G/U, R=A/G, H=A/C/U) sequence motifs at certain locations within RNA polymerase II transcripts.<sup>7-8</sup> Additionally, more structure- or sequence-specific  $m^6A$  writers have been characterized, including ZCCHC4,<sup>9</sup> METTL16,<sup>10-11</sup> METTL5,<sup>12</sup> PCIF1/CAPAM.<sup>13</sup> The methyl group attached to the exocyclic amino group at position 6 of adenosine can be located in *syn* or *anti* orientation with respect to the N1 in the purine ring (Figure 1A). While the *syn* orientation is energetically preferred in the free nucleosides and in single-stranded RNA, formation of a standard Watson-Crick base pair requires the methyl group to rotate into the *anti* conformation.<sup>14-16</sup> Thus,  $m^6A$  influences local structures and base-pairing kinetics, which in turn affect global RNA folding, structures and associated functions. Multiple studies have shown that  $m^6A$  modulates the fate of mRNAs by influencing their stability, translation efficiency, and splicing through direct or indirect interaction with proteins.<sup>2-3, 17-18</sup> A group of direct  $m^6A$  reader proteins each contain the YTH domain, which forms a hydrophobic binding pocket for  $m^6A$ . Well-established human  $m^6A$  readers include the proteins YTHDF1/DF2/DF3 and YTHDC1/DC2.<sup>18</sup> Although these YTH-domain containing proteins seem to bind  $m^6A$ -containing RNA via similar mechanisms, they

cause different downstream effects.<sup>19-20</sup> Interestingly,  $m^6A$  can be reverted to adenosine through oxidative demethylation by the human  $m^6A$  demethylase enzymes FTO and ALKBH5.<sup>4</sup> Both enzymes belong to the family of non-heme iron(II)- and  $\alpha$ -ketoglutarate-dependent dioxygenases but remove the  $N^6$ -methyl group via distinct reaction pathways: while demethylation by ALKBH5 directly yields adenosine accompanied by release of formaldehyde,<sup>21-22</sup> the oxidized intermediates  $N^6$ -hydroxymethyladenosine ( $hm^6A$ ) and  $N^6$ -formyladenosine ( $f^6A$ ) have been observed in the FTO-mediated pathway (Figure 1A).<sup>23-24</sup> While ALKBH5 has been observed to remove only internal  $m^6A$ , preferably in DRACH motifs, FTO has also been shown to act on  $m^6A_m$ ,  $m^1A$ ,  $m^3U$  and  $m^3T$ .<sup>25-28</sup> The dysregulation of  $m^6A$  and associated writer, reader and eraser proteins has been connected to tumor development and disease. Therefore,  $m^6A$ -modifying proteins have gained increasing attention as targets for drug development.<sup>29</sup> The design of chemical inhibitors requires knowledge of specific interactions between RNA and proteins. Such insights can be derived from crystal structures in combination with molecular dynamics simulations,<sup>29-30</sup> and are supported by biochemical data obtained with mutated proteins, in which key functional amino acids in the active site are exchanged, e.g. by replacement with alanine. Introducing smaller changes by exchanging single functional groups via incorporation of artificial amino acids is more challenging (e.g. via stop-codon suppression). On the other hand, single atom exchanges on the nucleoside level can be introduced into synthetic oligonucleotides by solid-phase synthesis. Atomic mutagenesis of nucleosides is a very powerful strategy for biochemical investigations and

has been successfully used for the detailed analyses of ribozyme mechanisms,<sup>31-34</sup> including the ribosome,<sup>35-36</sup> but has barely been used for modified nucleosides or the analysis of RNA-protein interactions.

Here we introduce atomic mutagenesis of m<sup>6</sup>A to analyze the contributions of hydrogen bonding and electrostatic interactions between m<sup>6</sup>A-modified RNA and reader as well as eraser proteins. We synthesized a series of RNA oligonucleotides containing atomic mutants of m<sup>6</sup>A to examine RNA binding, enzyme activity and product distribution. The endocyclic nitrogen atoms at position 1, 3 and 7 of the purine ring were individually replaced by a CH group, yielding 1-deaza, 3-deaza and 7-deaza-N<sup>6</sup>-methyladenosine, respectively (Figure 1B). This study revealed insights into the sensitivity of reader and eraser proteins to atomic mutagenesis of their substrates. Interestingly, we found distinct differences between the dioxygenases FTO and ALKBH5, and also among individual, yet apparently similar, YTH domains. Our results also suggest c<sup>7</sup>m<sup>6</sup>A as a structurally neutral probe for m<sup>6</sup>A readers that is more resistant to demethylation than native m<sup>6</sup>A.

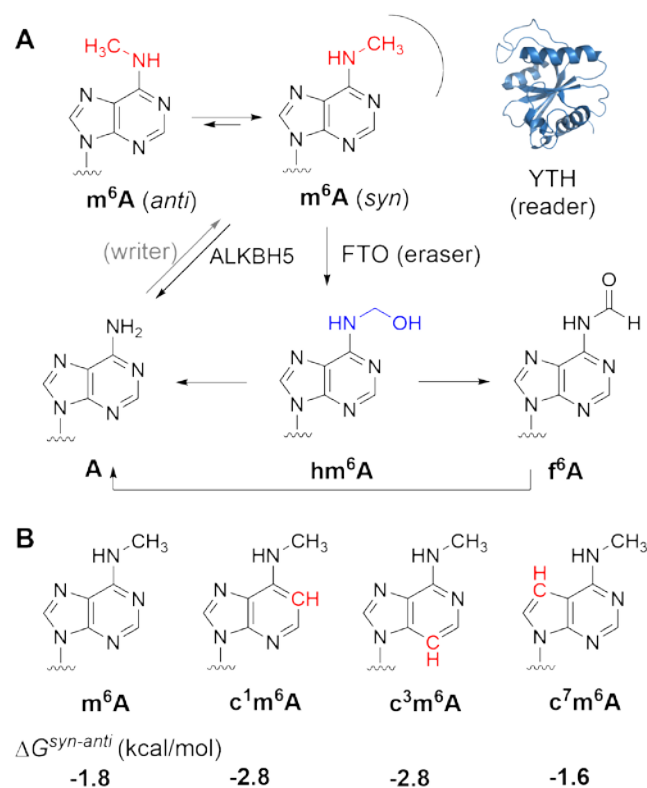


**Figure 1.** A) N<sup>6</sup>-methyladenosine (m<sup>6</sup>A) in Watson-Crick-competent *anti* orientation and protein-binding-competent *syn* conformation is installed by writer enzymes; m<sup>6</sup>A is removed by eraser enzymes (ALKBH5, FTO), and interacts with reader proteins (containing a YTH domain). B) m<sup>6</sup>A and the three deaza m<sup>6</sup>A mutants used in this study. The predicted free energy preference for the *syn* conformation is indicated.

## Results and Discussion

**Synthesis and Characterization.** The m<sup>6</sup>A nucleoside (**1a**) was obtained by nucleophilic substitution of 6-chloropurine riboside with methylamine as previously described.<sup>37-38</sup> Similarly, three deaza variants of m<sup>6</sup>A, c<sup>1</sup>m<sup>6</sup>A (**1b**), c<sup>3</sup>m<sup>6</sup>A

(**1c**) and c<sup>7</sup>m<sup>6</sup>A (**1d**) were prepared from suitable 6-chloro-substituted nucleoside analogs by substitution with methylamine. The required precursors were obtained by ribosylation of the respective nucleobase analogs under Silyl-Hilbert-Johnson conditions. The 1-deaza and 3-deaza purine analogs were obtained from 2-amino-4-chloropyridine (for **1b**) or 4-amino-2-chloropyridine (for **1c**), while 6-chloro-7-iodo-7-deazapurine was used for **1d** (Figure 2). The non-methylated nucleosides (c<sup>1</sup>A, c<sup>3</sup>A, c<sup>7</sup>A) were also prepared; details of the synthetic steps are given in the Supporting Information. The choice of the respective 2'-silyl protecting group was inspired by previous work on deazaadenosines.<sup>39-40</sup> The m<sup>6</sup>A nucleosides **1a-d** exhibit distinctly red-shifted UV absorption spectra (Figure S1, Table S1) compared to the respective unmethylated (deaza)adenosines. Moreover, the 1-deaza and 3-deaza analogues exhibit methylation-dependent changes in fluorescence emission intensity (Figure S2). DFT-based geometry optimization predicts the *syn* orientation of the methyl group as the energetically preferred conformation (Figure 1B, Figure S3), consistent with previously reported experimental data for m<sup>6</sup>A.<sup>41</sup>

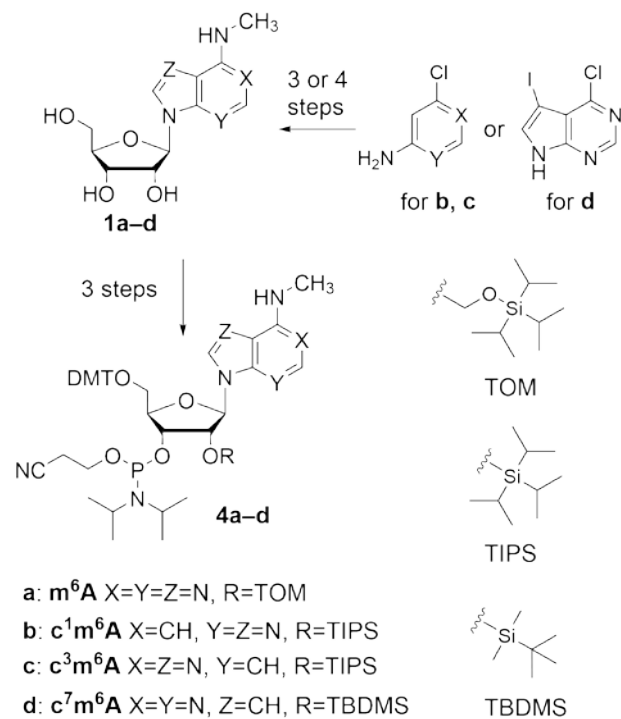


**Figure 2.** Synthesis of nucleosides and phosphoramidite building blocks for incorporation of m<sup>6</sup>A and its deaza mutants. Details of synthetic steps are in the Supporting Information. DMT = 4,4'-dimethoxytrityl, TOM = triisopropylsilyloxymethyl, TIPS = triisopropylsilyl, TBDMS = t-butyldimethylsilyl.

The free nucleosides **1a-d** were converted to the respective phosphoramidite building blocks **4a-d** in three steps, involving installation of 5'-DMT and 2'-silyl protecting groups, followed by 3' phosphorylation (Figure 2). These building blocks were used to incorporate the m<sup>6</sup>A variants into 12-mer oligonucleotides by solid phase synthesis using standard coupling and deprotection protocols. Each m<sup>6</sup>A analogue was installed in place of X in the sequence Hex-AACCGGX<sub>1</sub>CUGUC (**R1**: X=m<sup>6</sup>A, **R2**: X=c<sup>1</sup>m<sup>6</sup>A, **R3**: X=c<sup>3</sup>m<sup>6</sup>A,

**R4:** X=c<sup>7</sup>m<sup>6</sup>A, **R5:** X=A), thereby placing the m<sup>6</sup>A mutants inside a DRACH motif (underlined); RNAs were analyzed by HPLC and ESI-MS (Figure S4, Table S2); Hex denotes a hexynyl linker attached at the 5'-end for fluorescent labeling of the RNA using copper(I)-catalyzed azide-alkyne cycloaddition with fluorescein azide.

**Table 1. Thermal melting of 12-mer RNA duplexes containing N<sup>6</sup>-methylated adenosine derivatives and pK<sub>a</sub> of free nucleosides.**

RNA	A	T <sub>m</sub> [°C] <sup>a</sup>	ΔT <sub>m</sub> [°C] <sup>b</sup>	ΔG° [kcal/mol]	pK <sub>a</sub> <sup>c</sup>
<b>R1</b>	m <sup>6</sup> A	63.4	-2.8/0	-15.8	4.0 <sup>42-43</sup>
<b>R2</b>	c <sup>1</sup> m <sup>6</sup> A	53.9	-12.3/-9.5	-12.9	4.9 (4.7 <sup>44</sup> )
<b>R3</b>	c <sup>3</sup> m <sup>6</sup> A	58.7	-7.5/-4.7	-14.2	7.1 (6.8 <sup>44</sup> )
<b>R4</b>	c <sup>7</sup> m <sup>6</sup> A	62.9	-3.3/-0.5	-15.5	5.3 (5.2 <sup>44</sup> )
<b>R5</b>	A	66.2	0/+2.8	-16.2	3.6 <sup>42,45</sup>

<sup>a</sup> Determined by absorbance at 260 nm, for 5 μM RNA duplex with complementary **R6** 5'GACAGUCCGGU3'; (error ±0.5 °C).  
<sup>b</sup> Difference relative to the unmodified duplex/m<sup>6</sup>A-modified duplex, respectively. <sup>c</sup>pK<sub>a</sub> of free nucleoside (unmethylated deazaadenosine in parentheses).

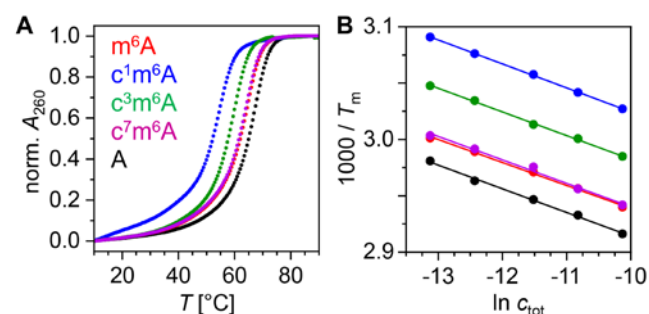


**Figure 3.** A) Melting curves (at 5 μM) and B) van't Hoff plots for RNA duplexes R1/R6 (m<sup>6</sup>A), R2/R6 (c<sup>1</sup>m<sup>6</sup>A), R3/R6 (c<sup>3</sup>m<sup>6</sup>A), R4/R6 (c<sup>7</sup>m<sup>6</sup>A), R5/R6 (unmodified A), (1, 2, 5, 10, 20 μM duplex), measured at 260 nm in 100 mM NaCl, 10 mM Na-phosphate buffer pH 7.0.

The base pairing properties of m<sup>6</sup>A and its deaza analogs in RNA duplexes was analyzed by thermal melting and van't Hoff analysis. The 12-mer RNAs **R1-R5** were hybridized to the complementary RNA **R6** and thermal denaturation was monitored by UV absorbance at 260 nm (Figure 3, Table S3, Figure S5). Consistent with previous reports, m<sup>6</sup>A slightly destabilized the duplex by less than one kcal/mol.<sup>15-16</sup> Replacing the N1 atom by carbon impaired Watson-Crick base pairing and resulted in a large drop of the T<sub>m</sub> by 9.5 °C compared to m<sup>6</sup>A. Replacing the N3 atom in the minor groove resulted in a reduced T<sub>m</sub> by 4.7 °C, while removing the N7 atom in the major groove had a negligible effect of only 0.5 °C. These melting data are consistent with the effects of deaza adenosines on RNA base pairing, where the destabilizing effect of c<sup>3</sup>A was attributed to its shifted pK<sub>a</sub> value and an altered hydration pattern in the minor groove.<sup>45-46</sup> To evaluate the influence of the methyl group on N<sup>6</sup>, we

determined the pK<sub>a</sub> of c<sup>3</sup>m<sup>6</sup>A (**1c**) and found it similarly shifted to neutrality (Figure S6, Table 1, Table S4). Thus, N1 of c<sup>3</sup>m<sup>6</sup>A is partially protonated at pH 7, reducing its Watson-Crick base pairing ability and resulting in the reduced T<sub>m</sub> of the **R3/R6** duplex. The higher predicted energetic preference of the *syn* conformation of c<sup>1</sup>m<sup>6</sup>A and c<sup>3</sup>m<sup>6</sup>A compared to m<sup>6</sup>A and c<sup>7</sup>m<sup>6</sup>A may also contribute to the lower T<sub>m</sub> of **R2/R6** and **R3/R6** duplexes.

Demethylation of m<sup>6</sup>A and its atomic mutants by FTO and ALKBH5

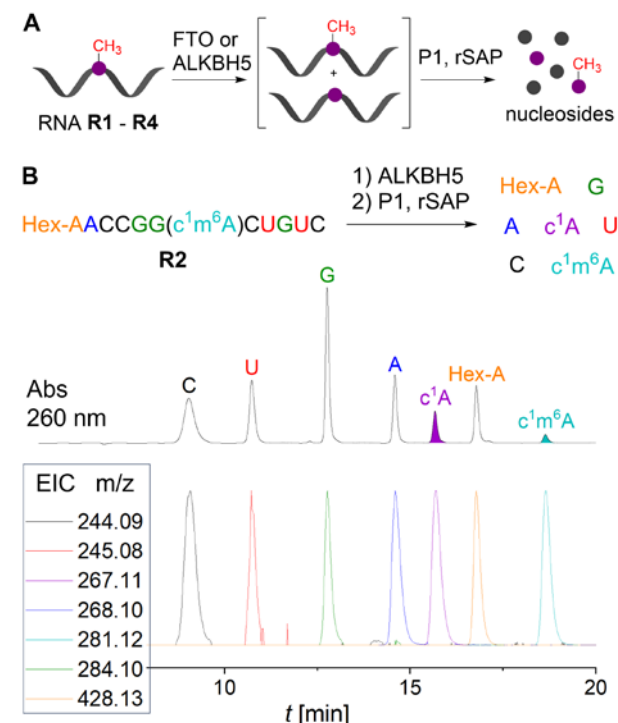


**Figure 4.** A) Schematic illustration of m<sup>6</sup>A demethylation assay. B) Exemplary data for R2 treated with ALKBH5 for 2 min. The signals in the UV absorbance trace are assigned to the nucleoside species based on the respective extracted ion chromatograms (EIC, m/z ±0.01). The extent of demethylation is calculated based on the respective integrated peak area (cyan and purple shade), using ε<sup>260</sup> of the free nucleosides.

Next, we used the oligonucleotides **R1-R4** to investigate the influence of m<sup>6</sup>A atomic mutagenesis on the enzymatic activity of the human m<sup>6</sup>A demethylases FTO and ALKBH5. **R1-R4** were incubated with recombinantly expressed and purified enzymes (see supporting information for details) in a buffer containing Fe(II) and α-ketoglutarate (α-KG) at 25 °C.<sup>47</sup> After digestion using Nuclease P1 and recombinant Shrimp Alkaline Phosphatase (rSAP), the obtained nucleoside mixtures were subsequently analyzed by HPLC-MS (Figure 4). The nucleosides were identified based on the ESI mass spectra and quantified based on the UV absorption at 260 nm, using the experimentally determined extinction coefficients of the respective nucleosides.

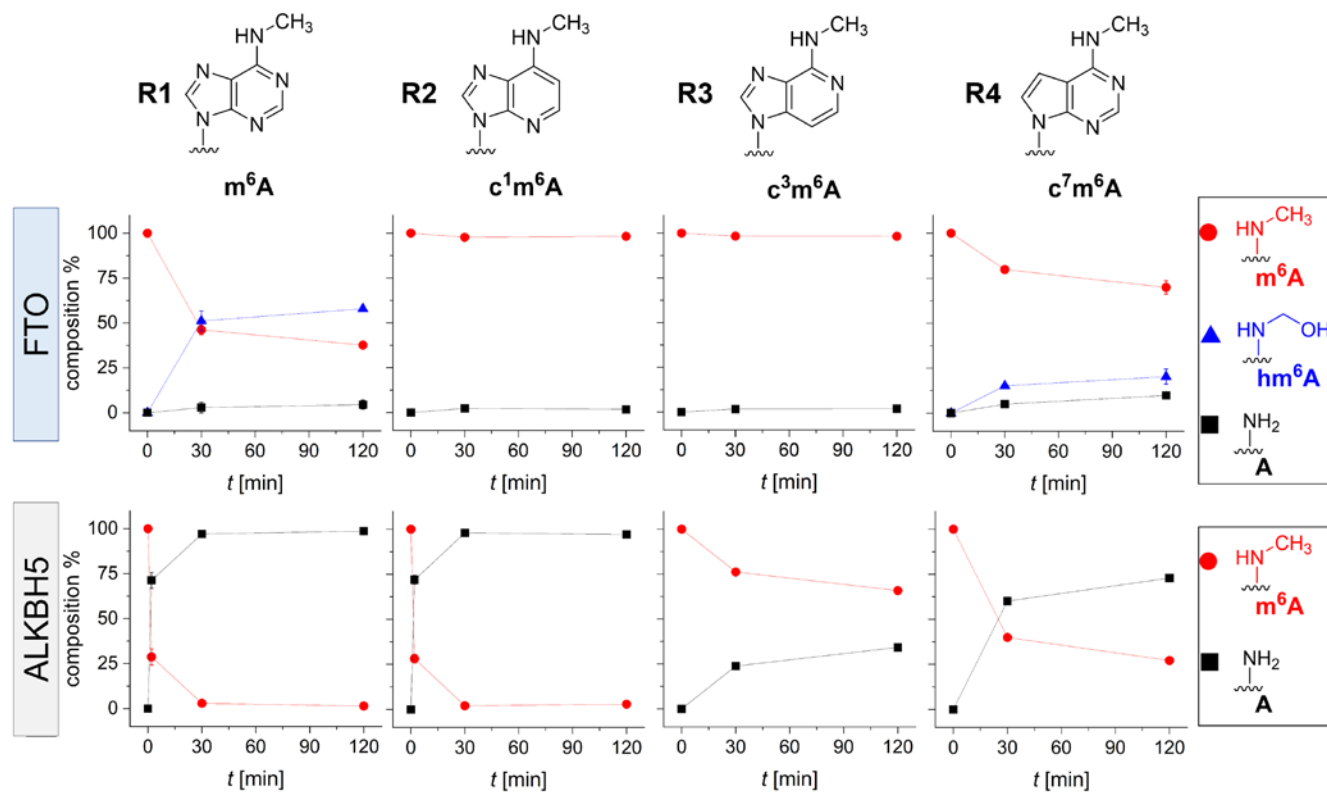


**Figure 5.** Product distribution obtained from oxidative demethylation of m<sup>6</sup>A analogs with FTO or with ALKBH5. All data points were collected as duplicates and are represented as mean ± s.e.m.

Details of the analysis are described in the Supplementary Information. The product distribution was analyzed at various time points, and the data are presented in Figure 5. Raw data for two independent replicates are shown in Figures S7-S10 and Tables S5-S8.

Treatment of **R1** with FTO or with ALKBH5 resulted in removal of the methyl group from m<sup>6</sup>A, as expected.<sup>4,21-24</sup> While FTO converted m<sup>6</sup>A to the oxidized intermediate hm<sup>6</sup>A and unmethylated A (58% and 4.5%, respectively, after 2 h), hm<sup>6</sup>A was not detected in the reaction with ALKBH5, which resulted in 71% demethylated product already after 2 min and nearly quantitative conversion after 30 min. These results are consistent with a previous report showing higher *in vitro* activity of ALKBH5 than FTO.<sup>21</sup>

Interestingly, ALKBH5 and FTO showed remarkably different results for demethylation of the atomic mutants. FTO did not tolerate the removal of either N1 or N3. The enzyme was essentially inactive on **R2** (c<sup>1</sup>m<sup>6</sup>A) and **R3** (c<sup>3</sup>m<sup>6</sup>A). Introduction of c<sup>7</sup>m<sup>6</sup>A into the oligonucleotide (**R4**) also decreased the demethylation efficiency of FTO (50% less conversion after 2 h compared to m<sup>6</sup>A); besides formation of unmethylated c<sup>7</sup>A (9.8% after 2 h), accumulation of the oxidized intermediate c<sup>7</sup>hm<sup>6</sup>A (20.3%) was observed.

ALKBH5 displayed markedly higher tolerance toward atomic mutagenesis of the endocyclic nitrogen atoms than FTO. Most notably, **R2** (c<sup>1</sup>m<sup>6</sup>A) was demethylated just as efficiently (ca. 72% demethylation after 2 min) as the native m<sup>6</sup>A substrate **R1**. This presents a major difference compared to FTO, which showed no activity on the c<sup>1</sup>m<sup>6</sup>A

substrate. RNAs containing c<sup>3</sup>m<sup>6</sup>A (**R3**) and c<sup>7</sup>m<sup>6</sup>A (**R4**) substrates were also accepted by ALKBH5, although demethylation occurred less efficiently (34% and 73% demethylation after 2 h, respectively), and oxidized intermediates were also not observed.

A previous study by Toh *et al.* traced the lack of oxidized m<sup>6</sup>A intermediates during ALKBH5-mediated demethylation back to a covalent intermediate in the enzymatic demethylation mechanism.<sup>21</sup> The authors visualized the covalent intermediate as a supershifted band in an electrophoretic mobility shift assay. We reproduced this result and found an analogous covalent ALKBH5-RNA adduct in the case of c<sup>7</sup>m<sup>6</sup>A demethylation (Figure S11). Of note, stabilization of the covalent adduct is achieved by pre-oxidation of the methylated RNA substrate by FTO (see Supplementary Information for experimental details). As c<sup>1</sup>m<sup>6</sup>A and c<sup>3</sup>m<sup>6</sup>A are not substrates of FTO, stabilization of **R2**-ALKBH5 and **R3**-ALKBH5 covalent adducts was not possible.

To examine if m<sup>6</sup>A atomic mutagenesis impairs recognition (binding) of the substrate oligonucleotides rather than enzymatic activity, we performed a competitive demethylation assay in which FTO or ALKBH5 were challenged with either only **R1**, or with a mixture of **R1** with either **R2**, **R3** or **R4**. In this experiment, m<sup>6</sup>A demethylation would be reduced compared to the **R1**-only sample if the present competitor RNA is bound by the demethylase. Indeed, for both enzymes we observed reduced m<sup>6</sup>A demethylation in the presence of **R2**-**R4** (Figures S12,13, Table S9), in each case to a similar extent. However, addition of **R5** had a

comparable effect, suggesting that FTO and ALKBH5 bind DRACH motifs regardless of the methylation status or the absence or presence of N1/N3/N7. Thus, these qualitative data support the interpretation of the demethylation results in Figure 5 as effects on catalysis rather than binding.

Overall, our systematic demethylation study provides comprehensive information about the molecular interactions responsible for accommodation of the m<sup>6</sup>A substrate inside the catalytic centers of FTO and ALKBH5. These data are largely consistent with available crystal structures (Figure 6).<sup>22, 48</sup> Hydrogen-bond interactions of N1 and N<sup>6</sup> of m<sup>6</sup>A with charged amino acid residues in the FTO catalytic site (R96 and E234) are crucial for the alignment of the N<sup>6</sup>-methyl group with the catalytic Fe(IV)-oxo center. Disruption of these interactions, as for the 1-deaza substrate, results in misorientation of the nucleobase and thus loss of catalytic activity. N7, in contrast, is not involved in stabilizing interactions and is therefore not crucial for m<sup>6</sup>A demethylation. Interestingly, the crystal structure of the FTO-m<sup>6</sup>A complex<sup>48</sup> does not indicate substrate-enzyme interactions involving the N3 of m<sup>6</sup>A, while atomic mutagenesis of this position caused a complete loss of enzymatic activity. We rationalize this observation with the protonation state of c<sup>3</sup>m<sup>6</sup>A due to its elevated pK<sub>a</sub> of 7.1, suggesting that electrostatic repulsion between a protonated N1 and the cationic side chain of R96 leads to misalignment of the c<sup>3</sup>m<sup>6</sup>A nucleobase in the catalytic site. Inside the ALKBH5 active site, N7 of the m<sup>6</sup>A substrate is not involved in electrostatic interactions; hence, the enzyme tolerates c<sup>1</sup>m<sup>6</sup>A as a substrate, and also maintains activity for demethylation of c<sup>3</sup>m<sup>6</sup>A. In addition, hydrogen bonding between N7 and the K132 side chain appears to contribute to correct substrate alignment and supports demethylation.

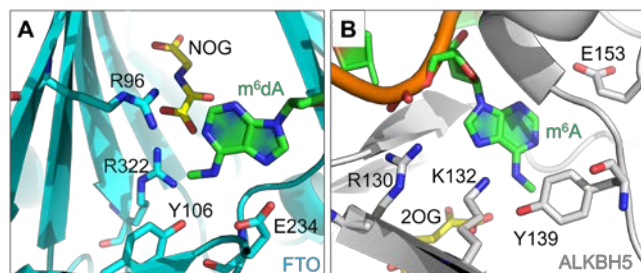


**Figure 6.** View into the active site of A) FTO (pdb 5zmd) and B) ALKBH5 (pdb 7wkv).

#### Binding of m<sup>6</sup>A mutants by YTH domain reader proteins

Next, we investigated recognition of the m<sup>6</sup>A atomic mutants by human YTH domain-containing m<sup>6</sup>A reader proteins. We used recombinantly expressed and purified YTHDF2<sup>380-579</sup>, YTHDC1<sup>344-509</sup> and YTHDC2<sup>1277-1430</sup> (in the following referred to as YTHDF2, YTHDC1 and YTHDC2) and the fluorescently labeled substrate oligonucleotides **R1-FAM** – **R5-FAM** to determine the protein-RNA dissociation constants ( $K_D$ ) via fluorescence anisotropy (Figure 7, Table 2).

In agreement with previous reports, all three reader proteins bound the native m<sup>6</sup>A substrate **R1** with affinities in the micromolar to sub-micromolar range, and strongly preferred the methylated RNA **R1** over the unmethylated RNA

**R5**.<sup>49-50</sup> Introduction of the c<sup>1</sup>m<sup>6</sup>A mutation resulted in reduced binding affinities of **R2** by at least 50-fold compared to **R1** for YTHDF2 and YTHDC1; for the weakest m<sup>6</sup>A binder YTHDC2, c<sup>1</sup>m<sup>6</sup>A led to complete loss of binding. Interestingly, the c<sup>3</sup>m<sup>6</sup>A substrate was well tolerated by YTHDF2 ( $K_D = 0.10 \mu\text{M}$ , only 3-fold increase compared to m<sup>6</sup>A), whereas YTHDC1 and YTHDC2 did not bind **R3**. Moreover, all three YTH domain readers displayed high tolerance toward atomic mutagenesis of N7: **R4** with c<sup>7</sup>m<sup>6</sup>A showed only ca. 3-fold increased  $K_D$  values for each of the three proteins.

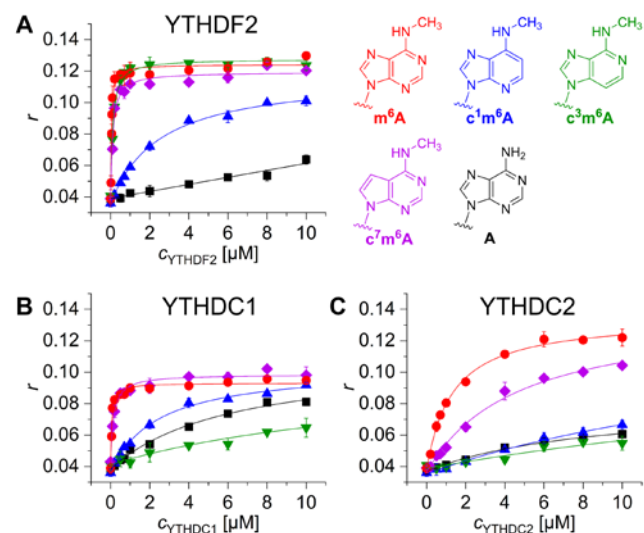


**Figure 7.** Binding isotherms of the (deaza)-m<sup>6</sup>A RNAs by reader proteins YTHDF2, YTHDC1 and YTHDC2, as determined by fluorescence anisotropy measurements via titration of 5'-FAM-labeled RNAs **R1-R5** (20 nM) with increasing concentrations of protein. All data points were collected as triplicates and are presented as mean  $\pm$  s.e.m.

**Table 2:** Dissociation constants of YTH protein-RNA complexes determined by fluorescence anisotropy.

RNA	$K_D$ [ $\mu\text{M}$ ]	$K_D$ [ $\mu\text{M}$ ]	$K_D$ [ $\mu\text{M}$ ]	
		YTHDF2	YTHDC1	YTHDC2
R1	m <sup>6</sup> A	0.035 $\pm$ 0.007	0.05 $\pm$ 0.01	1.3 $\pm$ 0.2
R2	c <sup>1</sup> m <sup>6</sup> A	2.5 $\pm$ 0.3	2.4 $\pm$ 0.3	n. d.
R3	c <sup>3</sup> m <sup>6</sup> A	0.10 $\pm$ 0.02	n. d.	n. d.
R4	c <sup>7</sup> m <sup>6</sup> A	0.10 $\pm$ 0.02	0.15 $\pm$ 0.03	4.6 $\pm$ 1.0
R5	A	n. d.	6.2 $\pm$ 1.5	n. d.

$K_D$  values are given as mean  $\pm$  s.e.m. of triplicates. In case of negligible binding at 10  $\mu\text{M}$  protein,  $K_D$  values were not determined (n. d.)

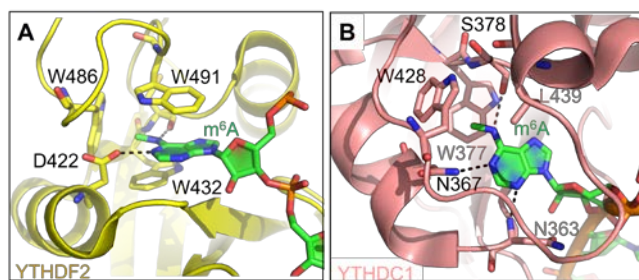


**Figure 8.** View into the binding site of A) YTHDF2 (pdb 7z26) and B) YTHDC1 (pdb 4r31).

These experimental observations correlate with previously reported crystal structures of  $m^6A$  bound to YTHDF2 and YTHDC1 (Figure 8).<sup>30,50</sup> These structures show the  $m^6A$  nucleobase located in an aromatic cage, which is stabilized by  $\pi$ - $\pi$ -stacking with tryptophan side chains located parallel to the purine heterocycle (W432 and W491 in DF2, and W377 in DC1), and a methyl- $\pi$  interaction with a tryptophan side chain that is located orthogonal to the  $N^6$ -methyl group (W486 in DF2 and W428 in DC1). The RNA-protein complexes are further stabilized by hydrogen bonding interactions of the N1 nitrogen of  $m^6A$  with a carboxyl group (D422) in YTHDF2, or with an amide (N367) in YTHDC1. The loss of these hydrogen bonds by using  $c^1m^6A$  is likely responsible for the drastically reduced affinity of **R2**. In case of the  $c^3m^6A$  mutant in **R3**, the elevated  $pK_a$  value and the concomitant partial N1 protonation likely prevents a stabilizing interaction with N367 in YTHDC1 (and in analogy with N1300 in YTHDC2). In contrast, YTHDF2 easily accommodates  $c^3m^6A$ , which is likely supported by an electrostatic attraction between aspartate and the positive N1 site, which cannot be achieved with the asparagine at the corresponding site in YTHDC1/2.

By contrast, N7 of  $m^6A$  is not involved in any direct interactions with amino acids in any of the YTH domains, and atomic mutagenesis of this site is therefore well tolerated. Together with the results from UV melting showing that  $c^7m^6A$  has very similar thermodynamic effects as  $m^6A$ , and the fact that it is much more slowly demethylated than  $m^6A$ , our data suggest  $c^7m^6A$  as a useful tool for further  $m^6A$  research.

## Conclusion

We have synthesized a series of deaza  $m^6A$  analogues and used them to systematically probe structural features for the recognition of  $m^6A$  by eraser and reader proteins. Individually replacing the nitrogen atom at position 1, 3 or 7 by a CH group resulted in the  $m^6A$  analogues  $c^1m^6A$ ,  $c^3m^6A$  and  $c^7m^6A$ . Upon incorporation into oligonucleotides, the destabilizing effect on Watson-Crick base pairing increased in the order  $m^6A \sim c^7m^6A < c^3m^6A < c^1m^6A$ .

HPLC-MS-based demethylation studies revealed that the enzymatic demethylation efficiency of human  $m^6A$  dioxygenases FTO and ALKBH5 was markedly affected by  $m^6A$  atomic mutagenesis. In the case of FTO-mediated demethylation, we identified N1 as a key structural feature that is engaged in electrostatic interactions with the enzyme active site to ensure proper alignment of the exocyclic substituent within the catalytic core. ALKBH5, by contrast, showed

tolerance toward all  $m^6A$  atomic mutants, although 7-deaza and 3-deaza mutations led to reduced demethylation efficiency. While FTO-mediated demethylation involves release of oxidized  $N^6$ -hydroxymethyl intermediates, ALKBH5 directly converts its substrates to their respective unmethylated products. Our experimental results support recent reports that this mechanistic discrepancy is based on a covalent demethylation mechanism of ALKBH5.

Further fluorescence spectroscopy-based investigations revealed that also  $m^6A$  recognition by its reader proteins YTHDF2, YTHDC1 and YTHDC2 relies on electrostatic interactions involving N1 in addition to the exocyclic methylamino group. Absence or (for YTHDC1 and YTHDC2) protonation of N1 led to drastically reduced binding affinities. Overall, our study provided valuable insights into the structural requirements for substrate recognition by  $m^6A$  reader proteins and demethylation events mediated by  $m^6A$  demethylases. The identification of crucial structural features and interactions may aid future research on these proteins as drug targets. Furthermore, the building blocks disclosed in this study may serve as useful probes for the investigation of other  $m^6A$ -interacting proteins that are involved in regulating  $m^6A$ -dependent cellular pathways.

## ASSOCIATED CONTENT

**Supporting Information.** Supplementary methods, NMR spectra of the synthesized compounds, UV/Vis and fluorescence spectra of the free nucleosides, anion exchange and ESI-MS data of the synthesized oligonucleotides, HPLC-MS raw data, geometry-optimized structures. This material is available free of charge via the Internet at <http://pubs.acs.org>.

## AUTHOR INFORMATION

Corresponding Author

\*claudia.hoebartner@uni-wuerzburg.de

## ACKNOWLEDGMENT

This work was supported by the Deutsche Forschungsgemeinschaft (DFG) via SPP1784 (project No 277312423), and SFB 1565 (project No 469281184, P12 to K.E.B. and P18 to C.H. and M.T.B.).

## REFERENCES

- Motorin, Y.; Helm, M., RNA nucleotide methylation: 2021 update. *Wiley Interdiscip Rev RNA* **2022**, *13*, e1691.
- Murakami, S.; Jaffrey, S. R., Hidden codes in mRNA: Control of gene expression by  $m(6)A$ . *Mol Cell* **2022**, *82*, 2236-2251.
- Delaunay, S.; Helm, M.; Frye, M., RNA modifications in physiology and disease: towards clinical applications. *Nat Rev Genet* **2024**, *25*, 104-22.
- Zaccara, S.; Ries, R. J.; Jaffrey, S. R., Reading, writing and erasing mRNA methylation. *Nat Rev Mol Cell Biol* **2019**, *20*, 608-624.
- Dominissini, D.; Moshitch-Moshkovitz, S.; Schwartz, S.; Salmon-Divon, M.; Ungar, L.; Osenberg, S.; Cesarkas, K.; Jacob-Hirsch, J.; Amariglio, N.; Kupiec, M.; Sorek, R.; Rechavi, G., Topology of the human and mouse  $m^6A$  RNA methylomes revealed by  $m^6A$ -seq. *Nature* **2012**, *485*, 201-6.
- Meyer, K. D.; Saletore, Y.; Zumbo, P.; Elemento, O.; Mason, C. E.; Jaffrey, S. R., Comprehensive Analysis of mRNA Methylation

- Reveals Enrichment in 3' UTRs and near Stop Codons. *Cell* **2012**, *149*, 1635-46.
7. Liu, J.; Yue, Y.; Han, D.; Wang, X.; Fu, Y.; Zhang, L.; Jia, G.; Yu, M.; Lu, Z.; Deng, X.; Dai, Q.; Chen, W.; He, C., A METTL3-METTL14 complex mediates mammalian nuclear RNA N<sup>6</sup>-adenosine methylation. *Nat Chem Biol* **2014**, *10*, 93-5.
  8. Schöller, E.; Weichmann, F.; Treiber, T.; Ringle, S.; Treiber, N.; Flatley, A.; Feederle, R.; Bruckmann, A.; Meister, G., Interactions, localization, and phosphorylation of the m(6)A generating METTL3-METTL14-WTAP complex. *RNA* **2018**, *24*, 499-512.
  9. Ma, H.; Wang, X.; Cai, J.; Dai, Q.; Natchiar, S. K.; Lv, R.; Chen, K.; Lu, Z.; Chen, H.; Shi, Y. G.; Lan, F.; Fan, J.; Klaholz, B. P.; Pan, T.; Shi, Y.; He, C., N(6)-Methyladenosine methyltransferase ZCCHC4 mediates ribosomal RNA methylation. *Nat Chem Biol* **2019**, *15*, 88-94.
  10. Warda, A. S.; Kretschmer, J.; Hackert, P.; Lenz, C.; Urlaub, H.; Höbartner, C.; Sloan, K. E.; Bohnsack, M. T., Human METTL16 is a N(6)-methyladenosine (m(6)A) methyltransferase that targets pre-mRNAs and various non-coding RNAs. *EMBO Rep* **2017**, *18*, 2004-2014.
  11. Satterwhite, E. R.; Mansfield, K. D., RNA methyltransferase METTL16: Targets and function. *Wiley Interdiscip Rev RNA* **2022**, *13*, e1681.
  12. van Tran, N.; Ernst, F. G. M.; Hawley, B. R.; Zorbas, C.; Ulryck, N.; Hackert, P.; Bohnsack, K. E.; Bohnsack, M. T.; Jaffrey, S. R.; Graille, M.; Lafontaine, D. L. J., The human 18S rRNA m6A methyltransferase METTL5 is stabilized by TRMT112. *Nucleic Acids Res* **2019**, *47*, 7719-7733.
  13. Sendinc, E.; Valle-Garcia, D.; Dhall, A.; Chen, H.; Henriques, T.; Navarrete-Perea, J.; Sheng, W.; Gygi, S. P.; Adelman, K.; Shi, Y., PCIF1 Catalyzes m6Am mRNA Methylation to Regulate Gene Expression. *Mol Cell* **2019**, *75*, 620-630 e9.
  14. Micura, R.; Pils, W.; Höbartner, C.; Grubmayr, K.; Ebert, M. O.; Jaun, B., Methylation of the nucleobases in RNA oligonucleotides mediates duplex-hairpin conversion. *Nucleic Acids Res* **2001**, *29*, 3997-4005.
  15. Roost, C.; Lynch, S. R.; Batista, P. J.; Qu, K.; Chang, H. Y.; Kool, E. T., Structure and Thermodynamics of N<sup>6</sup>-Methyladenosine in RNA: A Spring-Loaded Base Modification. *J Am Chem Soc* **2015**, *137*, 2107-15.
  16. Shi, H.; Liu, B.; Nussbaumer, F.; Rangadurai, A.; Kreutz, C.; Al-Hashimi, H. M., NMR Chemical Exchange Measurements Reveal That N(6)-Methyladenosine Slows RNA Annealing. *J Am Chem Soc* **2019**, *141*, 19988-19993.
  17. Jain, S.; Koziej, L.; Poulis, P.; Kaczmarczyk, I.; Gaik, M.; Rawski, M.; Ranjan, N.; Glatt, S.; Rodnina, M. V., Modulation of translational decoding by m(6)A modification of mRNA. *Nat Commun* **2023**, *14*, 4784.
  18. Höfler, S.; Duss, O., Interconnections between m6A RNA modification, RNA structure, and protein-RNA complex assembly. *Life Sci Alliance* **2024**, *7*.
  19. Roundtree, I. A.; Luo, G. Z.; Zhang, Z.; Wang, X.; Zhou, T.; Cui, Y.; Sha, J.; Huang, X.; Guerrero, L.; Xie, P.; He, E.; Shen, B.; He, C., YTHDC1 mediates nuclear export of N(6)-methyladenosine methylated mRNAs. *Elife* **2017**, *6*.
  20. Zaccara, S.; Jaffrey, S. R., A Unified Model for the Function of YTHDF Proteins in Regulating m(6)A-Modified mRNA. *Cell* **2020**, *181*, 1582-1595 e18.
  21. Toh, J. D. W.; Crossley, S. W. M.; Bruemmer, K. J.; Ge, E. J.; He, D.; Iovan, D. A.; Chang, C. J., Distinct RNA N-demethylation pathways catalyzed by nonheme iron ALKBH5 and FTO enzymes enable regulation of formaldehyde release rates. *Proc Natl Acad Sci USA* **2020**, *117*, 25284-92.
  22. Kaur, S.; Tam, N. Y.; McDonough, M. A.; Schofield, C. J.; Aik, W. S., Mechanisms of substrate recognition and N6-methyladenosine demethylation revealed by crystal structures of ALKBH5-RNA complexes. *Nucleic Acids Res* **2022**, *50*, 4148-4160.
  23. Fu, Y.; Jia, G.; Pang, X.; Wang, R. N.; Wang, X.; Li, C. J.; Smemo, S.; Dai, Q.; Bailey, K. A.; Nobrega, M. A.; Han, K. L.; Cui, Q.; He, C., FTO-mediated formation of N<sup>6</sup>-hydroxymethyladenosine and N<sup>6</sup>-formyladenosine in mammalian RNA. *Nat Commun* **2013**, *4*, 1798.
  24. Jia, G.; Fu, Y.; Zhao, X.; Dai, Q.; Zheng, G.; Yang, Y.; Yi, C.; Lindahl, T.; Pan, T.; Yang, Y. G.; He, C., N6-methyladenosine in nuclear RNA is a major substrate of the obesity-associated FTO. *Nat Chem Biol* **2011**, *7*, 885-7.
  25. Mauer, J.; Sindelar, M.; Despici, V.; Guez, T.; Hawley, B. R.; Vasseur, J. J.; Rentmeister, A.; Gross, S. S.; Pellizzoni, L.; Debart, F.; Goodarzi, H.; Jaffrey, S. R., FTO controls reversible m(6)Am RNA methylation during snRNA biogenesis. *Nat Chem Biol* **2019**, *15*, 340-347.
  26. Mauer, J.; Luo, X.; Blanjoie, A.; Jiao, X.; Grozhik, A. V.; Patil, D. P.; Linder, B.; Pickering, B. F.; Vasseur, J. J.; Chen, Q.; Gross, S. S.; Elemento, O.; Debart, F.; Kiledjian, M.; Jaffrey, S. R., Reversible methylation of m<sup>6</sup>A<sub>m</sub> in the 5' cap controls mRNA stability. *Nature* **2017**, *541*, 371-5.
  27. Wei, J.; Liu, F.; Lu, Z.; Fei, Q.; Ai, Y.; He, P. C.; Shi, H.; Cui, X.; Su, R.; Klungland, A.; Jia, G.; Chen, J.; He, C., Differential m<sup>6</sup>A, m<sup>6</sup>Am, and m<sup>1</sup>A Demethylation Mediated by FTO in the Cell Nucleus and Cytoplasm. *Mol Cell* **2018**, *71*, 973-985.
  28. Jia, G.; Yang, C. G.; Yang, S.; Jian, X.; Yi, C.; Zhou, Z.; He, C., Oxidative demethylation of 3-methylthymine and 3-methyluracil in single-stranded DNA and RNA by mouse and human FTO. *FEBS Lett* **2008**, *582*, 3313-9.
  29. Huang, Y.; Xia, W.; Dong, Z.; Yang, C. G., Chemical Inhibitors Targeting the Oncogenic m(6)A Modifying Proteins. *Acc Chem Res* **2023**, *56*, 3010-3022.
  30. Nai, F.; Nachawati, R.; Zalesak, F.; Wang, X.; Li, Y.; Caflisch, A., Fragment Ligands of the m(6)A-RNA Reader YTHDF2. *ACS Med Chem Lett* **2022**, *13*, 1500-1509.
  31. Egger, M.; Bereiter, R.; Mair, S.; Micura, R., Scaling Catalytic Contributions of Small Self-Cleaving Ribozymes. *Angew Chem Int Ed Engl* **2022**, *61*, e202207590.
  32. Micura, R.; Höbartner, C., Fundamental studies of functional nucleic acids: aptamers, riboswitches, ribozymes and DNAzymes. *Chem Soc Rev* **2020**, *49*, 7331-7353.
  33. Kosutic, M.; Neuner, S.; Ren, A.; Flur, S.; Wunderlich, C.; Mairhofer, E.; Vusurovic, N.; Seikowski, J.; Breuker, K.; Höbartner, C.; Patel, D. J.; Kreutz, C.; Micura, R., A Mini-Twister Variant and Impact of Residues/Cations on the Phosphodiester Cleavage of this Ribozyme Class. *Angew Chem Int Ed Engl* **2015**, *54*, 15128-15133.
  34. Bereiter, R.; Renard, E.; Breuker, K.; Kreutz, C.; Ennifar, E.; Micura, R., 1-Deazaguanosine-Modified RNA: The Missing Piece for Functional RNA Atomic Mutagenesis. *J Am Chem Soc* **2022**, *144*, 10344-10352.
  35. Lang, K.; Erlacher, M.; Wilson, D. N.; Micura, R.; Polacek, N., The role of 23S ribosomal RNA residue A2451 in peptide bond synthesis revealed by atomic mutagenesis. *Chem Biol* **2008**, *15*, 485-92.
  36. Clementi, N.; Chirkova, A.; Puffer, B.; Micura, R.; Polacek, N., Atomic mutagenesis reveals A2660 of 23S ribosomal RNA as key to EF-G GTPase activation. *Nat Chem Biol* **2010**, *6*, 344-51.
  37. Höbartner, C.; Kreutz, C.; Flecker, E.; Ottenschläger, E.; Pils, W.; Grubmayr, K.; Micura, R., The Synthesis of 2'-O-[(Triisopropylsilyl)oxy] methyl ( TOM ) Phosphoramidites of Methylated Ribonucleosides (m1G, m2G, m22G, m1I, m3U, m4C, m6A, m62A) for Use in Automated RNA Solid-Phase Synthesis. *Monatshfte für Chemie / Chemical Monthly* **2003**, *134*, 851-873.
  38. Sednev, M. V.; Mykhailiuk, V.; Choudhury, P.; Halang, J.; Sloan, K. E.; Bohnsack, M. T.; Hobartner, C., N(6)-Methyladenosine-Sensitive RNA-Cleaving Deoxyribozymes. *Angew Chem Int Ed* **2018**, *57*, 15117-15121.
  39. Neuner, S.; Falschlunger, C.; Fuchs, E.; Himmelstoss, M.; Ren, A.; Patel, D. J.; Micura, R., Atom-Specific Mutagenesis Reveals Structural and Catalytic Roles for an Active-Site Adenosine and

Hydrated Mg(2+) in Pistol Ribozymes. *Angew Chem Int Ed* **2017**, *56*, 15954-15958.

40. Mairhofer, E.; Fuchs, E.; Micura, R., Facile synthesis of a 3-deazaadenosine phosphoramidite for RNA solid-phase synthesis. *Beilstein J Org Chem* **2016**, *12*, 2556-2562.

41. Engel, J. D.; von Hippel, P. H., Effects of methylation on the stability of nucleic acid conformations: studies at the monomer level. *Biochemistry* **1974**, *13*, 4143-58.

42. Martin, M. G.; Reese, C. B., Some aspects of the chemistry of N(1)- and N(6)-dimethylallyl derivatives of adenosine and adenine. *J Chem Soc Perkin 1* **1968**, *14*, 1731-8.

43. Jones, E. L.; Mlotkowski, A. J.; Hebert, S. P.; Schlegel, H. B.; Chow, C. S., Calculations of pK(a) Values for a Series of Naturally Occurring Modified Nucleobases. *J Phys Chem A* **2022**, *126*, 1518-1529.

44. Itoh, T.; Kitano, S.; Mizuno, Y., Synthetic studies of potential antimetabolites. XIII. Synthesis of 7-amino-3-β-d-ribofuranosyl-3H-imidazo[4,5-b] pyridine (1-deazaadenosine) and related nucleosides. *J Heterocyclic Chem* **1972**, *9*, 465-470.

45. Krishnamurthy, R., Role of pK(a) of nucleobases in the origins of chemical evolution. *Acc Chem Res* **2012**, *45*, 2035-44.

46. Bereiter, R.; Himmelstoss, M.; Renard, E.; Mairhofer, E.; Egger, M.; Breuker, K.; Kreutz, C.; Ennifar, E.; Micura, R., Impact of 3-deazapurine nucleobases on RNA properties. *Nucleic Acids Res* **2021**, *49*, 4281-4293.

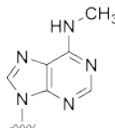
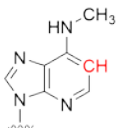
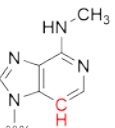
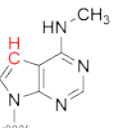
47. Haag, S.; Sloan, K. E.; Ranjan, N.; Warda, A. S.; Kretschmer, J.; Blessing, C.; Hubner, B.; Seikowski, J.; Dennerlein, S.; Rehling, P.; Rodnina, M. V.; Hobartner, C.; Bohnsack, M. T., NSUN3 and ABH1 modify the wobble position of mt-tRNA<sup>Met</sup> to expand codon recognition in mitochondrial translation. *EMBO J* **2016**, *35*, 2104-2119.

48. Zhang, X.; Wei, L. H.; Wang, Y.; Xiao, Y.; Liu, J.; Zhang, W.; Yan, N.; Amu, G.; Tang, X.; Zhang, L.; Jia, G., Structural insights into FTO's catalytic mechanism for the demethylation of multiple RNA substrates. *Proc Natl Acad Sci USA* **2019**, *116*, 2919-2924.

49. Kretschmer, J.; Rao, H.; Hackert, P.; Sloan, K. E.; Höbartner, C.; Bohnsack, M. T., The m(6)A reader protein YTHDC2 interacts with the small ribosomal subunit and the 5'-3' exoribonuclease XRN1. *RNA* **2018**, *24*, 1339-1350.

50. Xu, C.; Wang, X.; Liu, K.; Roundtree, I. A.; Tempel, W.; Li, Y.; Lu, Z.; He, C.; Min, J., Structural basis for selective binding of m6A RNA by the YTHDC1 YTH domain. *Nat Chem Biol* **2014**, *10*, 927-9.

## Table of Contents

				
	m <sup>6</sup> A	c <sup>1</sup> m <sup>6</sup> A	c <sup>3</sup> m <sup>6</sup> A	c <sup>7</sup> m <sup>6</sup> A
eraser	FTO	red	red	yellow
	ALKBH5	green	yellow	yellow
reader	YTHDF2	yellow	green	green
	YTHDC1	yellow	red	green
	YTHDC2	red	red	yellow
inhibition	no/low	medium	strong	